IGBT Remaining Useful Life Prediction Based on Transient Thermal Impedance

Jianwen Ge, Yixiang Huang, Zhiyu Tao, Chengliang Liu and Pengcheng Xia

***Abstract*- In motor drivers and wind energy converters, The insulated gate bipolar transistor (IGBT) is a vital electronic component. However, the IGBT is prone to failures such as bond wire lift-off and solder layer fatigue when working for a long time under high load conditions. Therefore, establishing a method to predict device failure in advance can reduce losses and assist maintenance. It is observed in the aging test that the transient thermal impedance changes with time. Therefore, this paper proposes a method for predicting the remaining useful life (RUL) using the features of the transient thermal impedance curve. Firstly, run-to-failure (RtF) aging tests are conducted to collect the temperature, the current, and the voltage to calculate the thermal impedance. Then, the features of the transient thermal impedance curve are extracted after data preprocessing. Finally, a deep neural network with attention mechanism is trained to predict RUL. The results show that the proposed method can accurately predict the RUL of the IGBT according to the change of the transient thermal impedance.[1]**

***Index Terms*- Insulated gate bipolar transistor (IGBT), remaining useful life (RUL), accelerated aging tests, power cycling (PC), transient thermal impedance, deep neural network (DNN), attention mechanism.**

I. Introduction

THE latest generation of IGBT not only has the significant advantages in terms of driving, such as high input impedance, low control power, and high switching speed, but also has the advantages in respect of output, such as high current density, low saturation voltage, and low switching loss. In application scenarios of high voltage, high current, and high frequency, IGBT has incomparable performance with other power devices. Therefore, IGBT becomes an ideal switching device in the field of power electronics. In motor drivers in electric vehicles and wind power converters in wind energy conversion, manufacturers mainly use IGBT as power devices[1, 2]. As a critical component of the electrical system, IGBT becomes the subject of many studies in recent years.

However, IGBT still has the problems of large internal impedance, large conduction consumption, and poor anti-shock capabilities when working under high voltage and high current. The statistical analysis of the reliability of industrial electronic devices shows that the power devices are the components that are most likely to fail in the electronic and electrical systems [2]. High load and temperature stress are the main causes of IGBT failure. 53% of IGBTs work at more than 80% of rated power, and about 14% of them are overloaded. The working temperature range of 38% IGBTs is 60 ~ 80 ℃, and that of 57% IGBTs is greater than 80 ℃ [2]. IGBT modules are stacked and welded by multi-layer materials with a significant difference in the coefficient of thermal expansion (CTE). When the temperature of IGBT changes, different CTEs between layers will result in huge stress. The periodical thermal stress will lead to the accumulation of stress fatigue in the welding joint, which will finally bring about failure.

The failure of IGBT will lead to the paralysis of the entire electrical system, the chain reaction of which may destroy the system and other related components. In many cases, the entire equipment will be shut down, which results in project postponement and economic loss of repairment. Therefore, it is urgent to build a reliable IGBT diagnosis system to predict the life of IGBT and to aid maintenance.

At present, mainstream approaches can be classified into three categories:

1) The finite element analysis (FEA) approaches based on the physical model[3, 4]. Thébaud, et al. [5] established a non-linear finite element simulation model to simulate the dissipated energy in solder to predict the failure of IGBT based on the energy theory that this part of the energy will act on the interior of the material and cause fatigue damage in each temperature cycle. However, FEA approaches need accurate parameters of the IGBT module and the cooling system to ensure the accuracy of the result. Astigarraga, et al. [6] and Ali, et al. [7] used IGBT modules of different manufacturers and types for the aging test. They found that under the same test conditions, the final failure modes of different modules were different and the changing trends of gate current, gate voltage, and collector voltage of different modules varied from module to module. These results indicate that the aging proceedings and results will be significantly different when the internal parameters of IGBT are different. Therefore, FEA approaches may be unfeasible in the real operation scenarios, where the accurate parameters of IGBT are difficult to obtain.

2) The analytic approaches based on the empirical Coffin-Manson formula. The analytic approaches predict RUL based

This work is supported by the National Key Technology R&D Program of China (No. 2017YFB1302004), and NSFC project (No. 51975356).

The authors are with the School of Mechanical Engineering, Shanghai Jiao Tong University at Minhang, Shanghai 200240 China (e-mail: gejianwen@sjtu.edu.cn; huang.yixiang@sjtu.edu.cn; taozhiyu@sjtu.edu.cn; chlliu@sjtu.edu.cn; xpc19960921@sjtu.edu.cn).

on coffin-Manson fatigue theory that the number of temperature aging cycles of materials is exponentially related to the junction temperature swing ΔT_j. Therefore, researchers[8-13] conduct many aging tests under different temperature swings to find the analytical formula between RUL and temperature. However, the analytic method needs a large number of experiments to ensure the accuracy of the result, which will take a tremendous amount of time.

3) The data-driven approaches based on aging precursor parameters. It is a more reliable and practical method to find an effective precursor to reflect the aging degree and predict the remaining life of IGBT. Therefore, many different aging parameters have been proposed. Among them, on-state collector-emitter voltage ($V_{ce,on}$) is the most widely used. However, different researchers used different $V_{ce,on}$ measurement methods, and obtained different results[6, 8-11, 14-18]. Alghassi, et al. [19] found that $V_{ce,on}$ gradually increased with the increase of aging times, while Patil, et al. [14] found that the collector-emitter voltage ($V_{ce,on}$) reduces with aging. Different experimental conditions and different types of IGBTs lead to different trends[6, 18]. Researchers also proposed some other aging parameters, such as gate current (I_g)[20], collector-emitter saturation voltage ($V_{ce,sat}$)[14, 21], gate threshold voltage ($V_{g,th}$)[6, 14, 18, 22]. Nevertheless, these aging parameters can only be measured in an experimental environment, because measuring these aging parameters requires changing the experimental circuit or changing the driving mode, which is impossible in practice.

In other studies [23-25], the thermal impedance is used as the aging precursor. However, the thermal impedance is a quantity that changes with time after the IGBT is turned on. To apply this time-dependent parameter to evaluate the aging degree, extracting features from the transient thermal impedance curve can be a feasible solution. Therefore, this paper proposes a method to predict RUL by using the transient thermal impedance curve when IGBT is turned on. Firstly, we collect temperature, current, and voltage data in the IGBT run-to-fail aging test. Then, the transient thermal impedance of the IGBT module is calculated and the effective features are extracted. Finally, an attention neural network based on the extracted features is trained to predict the RUL of the IGBT.

The paper is organized as follows. In Section II, the accelerated aging test, data collection method, and test results are described. Section III introduces the proposed method of life prediction, including data cleaning, feature extraction, attention model, and the rolling prediction method. Then Section IV shows the results of data preprocessing and life prediction results. Finally, conclusions and future work are discussed in Section V.

II. AGING TEST

A. Aging Test-Bed

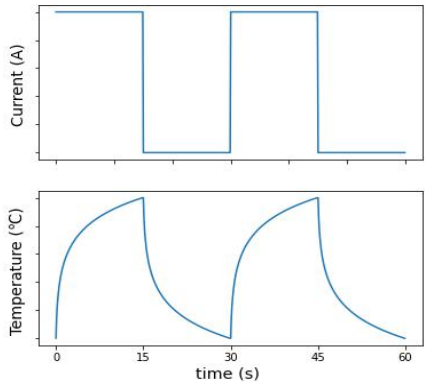

Fig. 1 DC aging cycle

An aging test is usually designed for analyzing the mechanism of degradation, identifying aging precursors, or verifying the temperature management strategy. Based on the heat source, aging tests can be divided into two classes: the thermal cycling test and the power cycling test. In the thermal cycling test, the device under test (DUT) is ensconced in a temperature control box and heated passively by the surrounded environment. In the power cycling test, DUT is heated by the thermal energy generated by the current flowing through the device. The temperature of the entire device simultaneously changes with the environment temperature in the thermal cycling test while a temperature distribution occurs in the power cycling test. Therefore, the power cycling test is more similar to the actual working condition. The power cycling test can be classified into two modes according to the form of the current: DC cycling and pulse width modulation (PWM) cycling. Because IGBTs are controlled by PWM voltage in practical work, it is more accurate to conduct PWM cycling. However, the thermal energy is mainly generated by on-state current instead of the lost energy in switching. Therefore, DC cycling can result in wider temperature swing and expedite the aging process. Fig.1 shows the DC cycling used in this paper. In every temperature cycle, DUTs are turned on for about 15 seconds heated by the current until the junction temperature (T_j) rises to the maximum temperature (T_{max}). Then, DUTs are turned off and cooled until T_j falls to the minimum temperature (T_{min}).

The test-bed for the aging test is shown in Fig. 2. The test-bed can be divided into three modules: the power cycle circuit, control system, and signal acquisition system. The DUT is an Infineon IGBT module FF50R12RT with a maximum rated voltage of 1200V and a maximum rated current of 50A. In this aging test-bed, one or more IGBT modules can be under test at the same time. The functions of the control system are drive control, temperature management, and data acquisition. The drive circuit is TX-DA962D6 which can control six IGBTs with a maximum output frequency of 60 kHz. A 0.47 μF absorption capacitance is connected in parallel with each IGBT to protect the IGBT from over-voltage and over-current. Four heat-resistant resistors are connected in series with the collector of the IGBT as the external load.

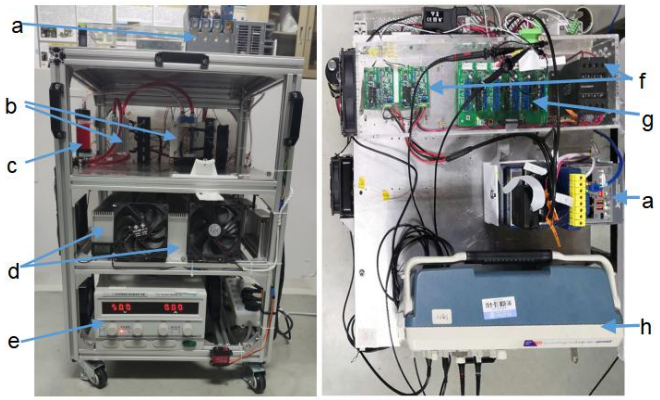

Fig. 2 Front view (left) and top view (right) of aging test-bed. (a) Control and acquisition system; (b) IGBTs; (c) Cooling system; (d) Resistors; (e) Power source;(f) Voltage transmitters; (g) Drive circuit; (h) Oscilloscope.

Fig. 3 illustrates the circuit of the power cycling test. The power cycling test circuit contains a voltage source, a switch, resistors, and IGBTs. Up to six IGBTs can be tested simultaneously. NI 9401 is used to control IGBTs by outputting PWM or DC voltage. The junction temperature and the package temperature of each IGBT are monitored by NI 9212 module. In the control program, we use the temperature acquired to determine whether to turn on or turn off DUTs so that these IGBTs work in a specific temperature swing (shown in Fig. 1). Also, a protected temperature is set to limit the maximum temperature.

B. Data Acquisition

In this paper, a run-to-failure (RtF) aging dataset in different temperature swing is collected to validate the proposed algorithm. In the aging test, the IGBT modules are operated at a high-temperature swing to accelerate the aging of IGBT. The test-bed not only collects the temperature of IGBT but also acquires the gate-emitter voltage V_{ge} and collector-emitter voltage V_{ce}.

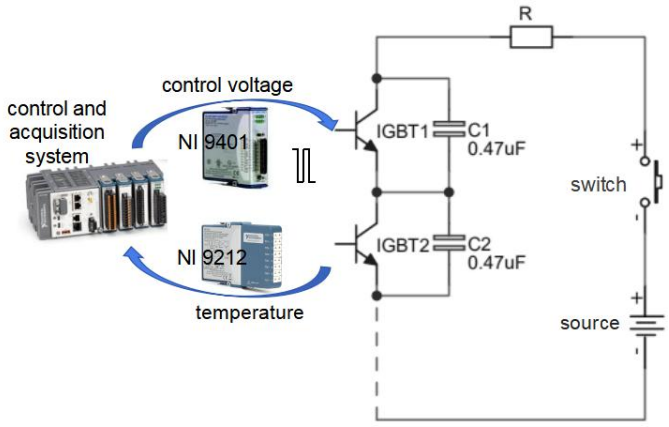

Fig. 3 The power cycling circuit.

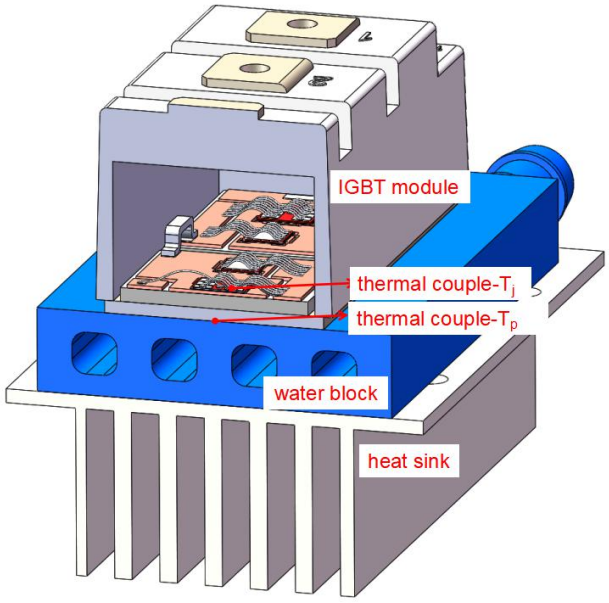

Fig. 4 Thermocouples of an IGBT module in sectional view.

The temperature acquisition diagram of the test-bed is shown in Fig. 4. Thermal couples with tiny welding joints are used to measure the temperature. A thermal couple is placed near the junction of bond wire to measure the junction temperature T_j and a thermal couple is inserted into the silicone grease between the IGBT module and water block to collect the package temperature T_p. The temperature is acquired in every 0.1s, which is the maximum sampling frequency.

In the experiment, two different voltage acquisition systems are applied to measure and monitor the voltage. One is a low-frequency signal acquisition system using NI 9234 as the acquisition module. V_{ge}, V_{ce}, and I_C which are scaled by the voltage transmitters and Hall current sensor are collected continuously at a lower frequency. This acquisition system is implemented in CompactRIO for real-time monitoring. The test will be instantly stopped if an exception such as a short circuit or open circuit occurs. Another set of acquisition systems utilizes Tektronix MSO 2014 oscilloscope to collect I_C, I_G, V_{GE}, and V_{ce} at a 0.5GHz sampling rate. In this paper, the data collected by the first acquisition system is used because we only need the on-state voltage and current to calculate the thermal impedance.

C. Experiment Result

TABLE I
EXPERIMENT RESULTS

Module	Duration (s)	T_{min} (°C)	T_{max} (°C)	ΔT (°C)	Lifetime (cycle)
IGBT1	30	90	170	80	67211
IGBT2		50	130		104092
IGBT3		40	120		148254
IGBT4		30	110		60492

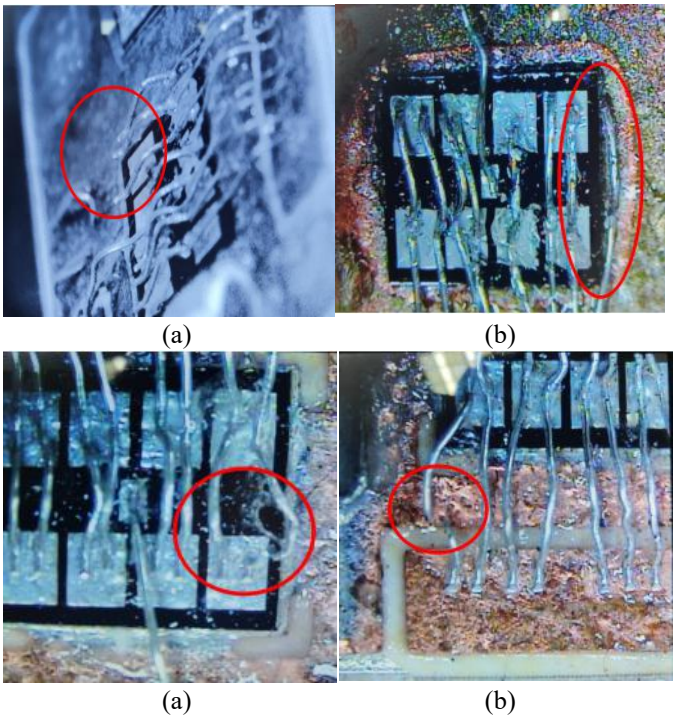

Fig. 5 Bond wire failures. (a) IGBT1 (b)IGBT2 (c) IGBT3 (4) IGBT4

On this test-bed, a total of four tests have been carried out aging the new intact IGBT module to fail. These modules are aged in different average temperatures, but they all work in the same temperature swing. The first IGBT is aged in the temperature range of 90 ℃ to 170 ℃, the second is 50 ℃ to 130 ℃, the third is 40 ℃ to 120 ℃, and the fourth is 30 ℃ to 110 ℃. The temperature range of these four tests is 80 ℃. In addition, the cycle period is the same. The lasting time of every temperature cycle is about 30 seconds.

Four IGBT modules all occurred bonding wire failure after about one month of aging. As is shown in Fig. 5, the bonding wires of IGBT1, IGBT2, and IGBT3 fall off, and the fourth IGBT module has broken bonding wires. Due to the difference in average temperature, the total aging cycle at failure is also different (see TABLE I). The first IGBT aging cycle is 67211 times, the second is 104092 times, the third is 148254, and the fourth is 60492 times. Many previous papers [8-13] have proved that the lower the temperature, the more aging cycles are required for the IGBT to fail. Therefore, IGBT2 and IGBT3 need more aging cycles than IGBT1. However, the fourth IGBT has fewer aging cycles than the first one because the IGBT module failed due to the fracture of the bonding wire. The fracture of the bonding wire during the test accelerated the aging process of the IGBT.

The obvious change that can be observed during the aging process is the increase of the transient thermal impedance of the IGBT module. Fig. 6 shows the transient thermal impedance curve of IGBT1 at the 40000th, 50000th, 55000th, 60000th, and 65000th temperature cycles. In the figure, the X-axis is the time after the IGBT turns on, and the Y-axis represents the thermal impedance of the IGBT module.

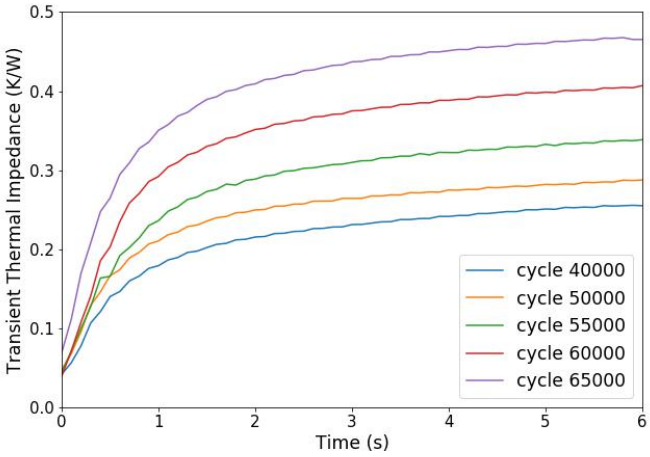

Fig. 6 Transient thermal impedance of the first IGBT in different cycles.

It can be observed that as the number of aging increases, the transient thermal impedance curve will rise to a higher level at a faster rate. Within one to six seconds after the IGBT is turned on, the larger the aging cycles, the greater the thermal impedance. When the IGBT is just turned on, the larger the aging cycles, the greater the slope of the thermal impedance curve. The transient thermal impedance of the other modules also shows a similar change. Therefore, the transient thermal impedance curve can reflect the aging degree of the IGBT.

III. Theory of RUL Prediction

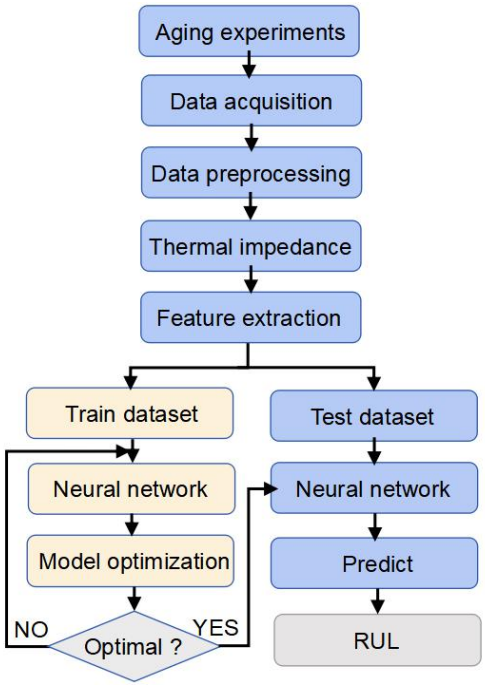

Fig. 7 Flow diagram of proposed RUL prediction method.

Fig. 7 shows the flow chart of the proposed RUL prediction method. Firstly, an accelerated aging test-bed is designed to obtain the data needed for the RUL prediction algorithm. Secondly, data filtering, outliers deleting, and signal denoising are conducted to acquire the informative data we are interested in. After further feature extraction, data sets for residual life prediction are obtained. After that, the data set is divided into a training dataset and a test set. An optimized neural network model is trained with the training set, and then the remaining life of the IGBT will be predicted.

A. Data preprocessing

There are inevitably some abnormal data in the dataset, which need to be eliminated first. Abnormal data mainly includes abnormal sensor signals and abnormal temperature cycles. Abnormal points in the signal collected by the sensor can be identified and deleted by comparing the difference between adjacent points in the signal. Because the temperature changes continuously, a temperature signal that suddenly increases or decreases is an abnormal point. The abnormal temperature cycle is caused by the failure of temperature control during the experiment preparation phase or closure phase. The cycle time of this kind of abnormal data is different from the normal data, and the maximum temperature and minimum temperature in a cycle are also far from the experimental conditions. Therefore, these data can be deleted by setting some thresholds.

B. Thermal Impedance

After getting the clean data, we can calculate the thermal impedance of the IGBT module by using the current, voltage, and temperature:

$$Z_{\mathrm{th}}(t) = (T_j(t) - T_p(t)) / (I_{ce} U_{ce,on}) \qquad (1)$$

where $Z_{th}(t)$ is the thermal impedance at time t. $T_j(t)$ and $T_p(t)$ are the junction temperature and package temperature at time t. I_{ce} and $V_{ce,on}$ are the current flowing through the IGBT collector and the conduction voltage across the collector and emitter.

The measurement and control of current, voltage, junction temperature, and package temperature have been described in Section II. The current Ice is constant in the experiment. The collector-emitter voltage changes slightly when the junction temperature changes, but the change is negligible compared to the temperature difference between the IGBT junction and the package. We are concerned about the thermal impedance change at the moment of IGBT turn-on, so we only calculate the thermal impedance during the 6 seconds after turn-on.

C. Feature Extraction

To measure the curve change of transient thermal impedance, we perform feature extraction on transient thermal impedance data. In this paper, we extract a total of 17 features. These features are shown in TABLE II.

These features reflect the characteristics of transient thermal impedance from different aspects. However, some characteristics do not reflect the relationship between thermal impedance and the number of aging cycles. Besides, features with too high correlation should be regarded as one feature and redundant features should be deleted to reduce the amount of calculation. This paper uses the correlation coefficient $\rho(\mathrm{X},\mathrm{Y})$ to analyze the correlation between different features and then deletes the features with higher correlation while retaining the features that are not highly correlated with each other but correlated with the cycle number. The correlation calculation formula is as follows:

$$\rho(\mathrm{X},\mathrm{Y}) = \sum_{i=1}^{\mathrm{N}} (\mathrm{X_i} - \mu_{\mathrm{X}})(\mathrm{Y_i} - \mu_{\mathrm{Y}}) \Big/ (\mathrm{N}\sigma_{\mathrm{X}}\sigma_{\mathrm{Y}}) \qquad (2)$$

where X and Y represent different feature serials. N is the length of the feature serial. μ_{X} and μ_{Y} are the mean values of X and Y respectively.

TABLE II
EXTRACTED FEATURES

Feature name	Formula
Mean	$\mu = \sum_{i=1}^{\mathrm{N}} \mathrm{s_i} \big/ \mathrm{N}$
Max	$\mathrm{Max} = \max(\mathrm{s_i})$
Min	$\mathrm{Min} = \min(\mathrm{s_i})$
Peak Value	$\mathrm{PV} = \max(\mathrm{s_i}) - \min(\mathrm{s_i})$
Variance	$\sigma^2 = \sum_{i=1}^{\mathrm{N}} (\mathrm{s_i} - \mu)^2 \big/ \mathrm{N}$
Standard Deviation	$\sigma = \sqrt{\sum_{i=1}^{\mathrm{N}} (\mathrm{s_i} - \mu)^2 \big/ \mathrm{N}}$
Root Mean Square	$\mathrm{RMS} = \sqrt{\sum_{i=1}^{\mathrm{N}} \mathrm{s_i}^2 \big/ \mathrm{N}}$
Kurtosis	$\mathrm{Kurt} = \sum_{i=1}^{\mathrm{N}} ((\mathrm{s_i} - \mu)/\sigma)^4 \big/ \mathrm{N} - 3$
Skewness	$\mathrm{Skew} = \sum_{i=1}^{\mathrm{N}} ((\mathrm{s_i} - \mu)/\sigma)^3 \big/ \mathrm{N}$
Mean of Absolute Value	$\mathrm{MAV} = \sum_{i=1}^{\mathrm{N}} \lvert \mathrm{s_i} \rvert \big/ \mathrm{N}$
Median Absolute Deviation	$\mathrm{MAD} = \mathrm{median}(\lvert s_i - \mathrm{median}(s_i) \rvert)$
Shape Factor	$\mathrm{SF} = \mathrm{RMS}/\mathrm{MAV}$
Impulse Factor	$\mathrm{IF} = \mathrm{Max}/\mathrm{MAV}$
Crest Factor	$\mathrm{CF} = \mathrm{PV}/\mathrm{RMS}$
Log-Log Ratio	$\mathrm{LLR} = \sum_{i=1}^{\mathrm{N}} \log(\lvert \mathrm{s_i} \rvert + 1) \big/ \log(\sigma)$
Log Energy Entropy	$\mathrm{LEE} = \sum_{i=1}^{\mathrm{N}} \log(\mathrm{s_i}^2)$
Shannon Entropy	$\mathrm{SE} = -\sum_{i=1}^{\mathrm{N}} \mathrm{s_i}^2 \log(\mathrm{s_i}^2)$

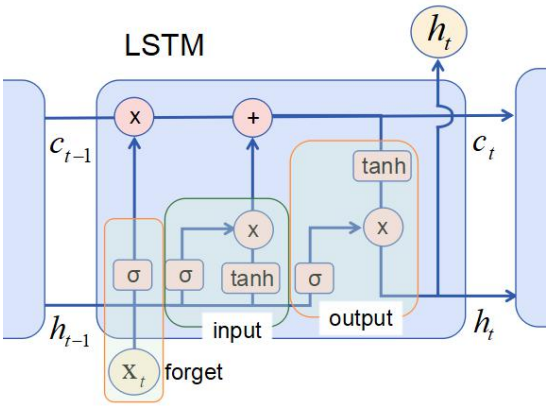

Fig. 8 LSTM. σ represents sigmoid function.

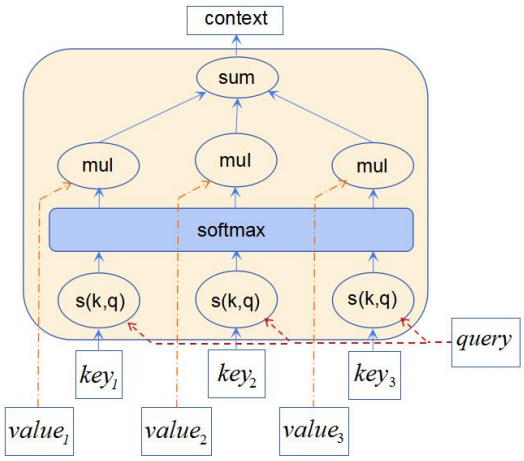

Fig. 9 Attention mechanism.

D. Long-Short Time Memory

The Long-Short Time Memory (LSTM)[26] is a classical type of the recurrent neural network (RNN), and have the ability to learn long-term dependency of a series. As shown in Fig. 8, the structure of LSTM is much more complex than that of RNN. These sophisticated connections enable LSTM to capture long-term dependency and avoid the problem of gradient vanishment and explosion which occur frequently when training RNN.

The structure of an LSTM cell is shown in Fig. 8. LSTM enhances the long term dependency by constructing three gates to control the information flow. The forget gate decides the amount of information to discard by the following formula:

$$f_t = sigmoid(W_f[h_{t-1}, x_t] + b_f) \tag{3}$$

where h_t and x_t are the hidden layer output of step t-1 and the input of step t which represent the information of previous steps and step t. f_t is the output is the forget gate. W_f and b_f are the parameters of the forget gate.

The input gate is designed to decide how much information should be added:

$$i_t = sigmoid(W_i[h_{t-1}, x_t] + b_i) \tag{4}$$

$$C_t = i_t * tanh(W_C[h_{t-1}, x_t] + b_C) + f_t * C_{t-1} \tag{5}$$

where W_C, b_C, W_i, and b_i are the parameters of the input gate. C_t and C_{t-1} are cell states of step t and step t-1.

Finally, the output gate calculates the hidden layer output by using C_t, h_t, and x_t:

$$o_t = sigmoid(W_o[h_{t-1}, x_t] + b_o) \tag{6}$$

$$h_t = o_t * tanh(C_{t-1}) \tag{7}$$

where W_o and b_o are the parameters of the input gate. h_t is the hidden state of step t.

E. Attention mechanism

Attention mechanism[27] has been widely and successfully applied in machine translation[28] and image recognition[29] in recent years. Compared with the traditional convolutional neural network (CNN) and RNN model, the attention network can get a better result because the attention mechanism makes the network focus on the specific part of the input image when processing images or align the output words with the input words when translating. When predicting RUL, the attention mechanism can also make the network pay more attention to the important time steps and features [30]. Therefore, in this paper, we improve the network by integrating the attention mechanism into the model.

As shown in Fig. 9, the attention network generates the attention context according to the inputs: query, key, and value. Firstly, we use matrix operation to adjust query **Q** and key $\mathbf{K_i}$ to the same dimension, and then calculate a score $s(\mathbf{Q}, \mathbf{K}_i)$ by multiplying parameter **v**.

$$s(\mathbf{Q}, \mathbf{K}_i) = v^T tanh(\mathbf{W}\mathbf{K}_i + \mathbf{U}\mathbf{Q}) \tag{8}$$

where **W** and **U** are the adjustment matrix of K and Q.

Then, the weight α_i is calculated by using the activate function to process the score:

$$\alpha_i = softmax(s(\mathbf{Q}, \mathbf{K}_i)) \tag{9}$$

Finally, the attention value $att(\mathbf{Q}, \mathbf{K}, \mathbf{V})$ is the sum of the dot product the weight and value:

$$att(\mathbf{Q}, \mathbf{K}, \mathbf{V}) = \sum_{i=1}^{N} \alpha_i \mathbf{V}_i \tag{10}$$

According to the equation, the main role of the attention network is to re-weight the value according to the query and the key. In different learning tasks, the value, the query, and the key are different. When the value is equal to the key or the value and the key are obtained from the same variable by matrix calculation, the attention model is called the self-attention model.

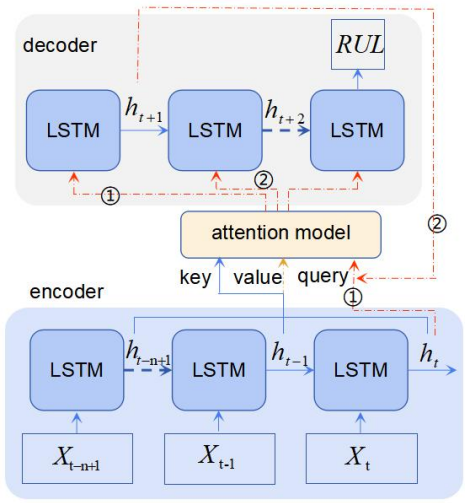

Fig. 10 RUL prediction model.

F. Prediction Model

The RUL prediction model with the attention mechanism is shown in Fig 10. The input of the model is the features of n time points before time t, and the output is the RUL of the IGBT module at time t. The model can be divided into three parts: encoder, decoder, and attention model. In the encoder, the input features X will first generate a hidden layer through an LSTM network. The hidden layer vector at each time point is input into the attention model as the key and value. Another input query **Q** of the Attention model is initialized by the hidden layer vector h_t that is the last output by the decoder. Then the hidden layer vector generated by the decoder is used as the value of the query. The output of the model is the last output of the LSTM in the decoder.

G. Rolling Prediction

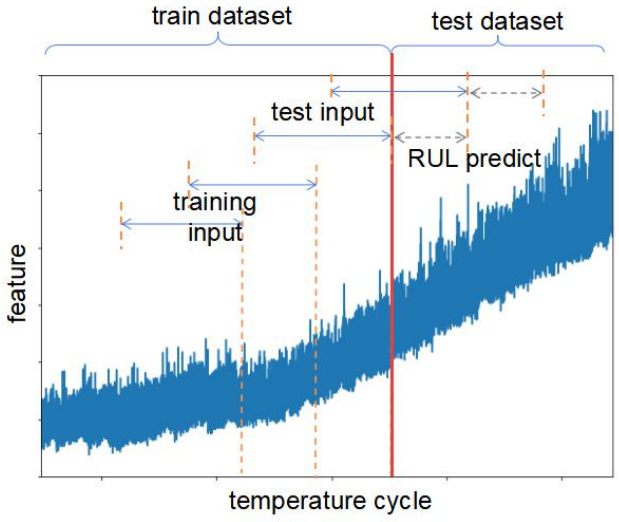

Fig. 11 Rolling prediction.

The rolling prediction method is used in this paper to predict the RUL (shown in Fig. 11). At the training step, all the train data is used to predict RUL and to train the model. However, at the prediction step, the data before time t is used to predict the remaining life of the next 200 time points. Then the data of these 200-time points are added to the training dataset to re-train the model. After that, the RUL of the next 200 time points after time t+200 can be generated by applying the re-trained model to the test data. Finally, the results of each prediction step are combined to obtain the predicted remaining life at each time point after time t. The pseudo-code is as follows:

begin
  Divide the data into train data and test data;
  Train prediction model using train data;
  for each t e test data **do begin**
    Predict RUL at time t;
    if 200 times prediction is finished **then begin**
      Add the part of data that have been used to train-data;
      Re-train the prediction model;
    end
  end
  return RUL
end

IV. RUL PREDICTION

A. Dataset

The data that has not been cleaned contains many abnormal values, which will seriously affect the accuracy of the life prediction algorithm. Fig.12 shows the features extracted directly from the transient thermal impedance curve without preprocessing. For the first IGBT, the trend of the feature with the number of aging cycles can be clearly observed, but several abnormal points seriously deviate from the normal trend. As for IGBT2, the changing trend becomes blurred due to the existence of abnormal points. Most of these abnormal points result from the abnormal cycle temperature that is not within the set range. For example, when the test-bed is starting, the temperature will start from environment temperature and the maximum temperature cannot reach the predetermined maximum temperature. There are also some abnormal points generated because the temperature acquisition sensor is interfered with, leading to the result that the collected temperature exceeds the set temperature range, and the temperature cycle ends or starts in advance. These incomplete temperature cycles will also cause the thermal resistance calculated to be different. Therefore, we delete these abnormal data by setting the threshold to the temperature and cycle time. For instance, in the dataset of the first IGBT, the cycles whose maximum temperature lower than 160 ℃, minimum temperature beyond 80 to 100℃, and cycle time less than 10 seconds are eliminated.

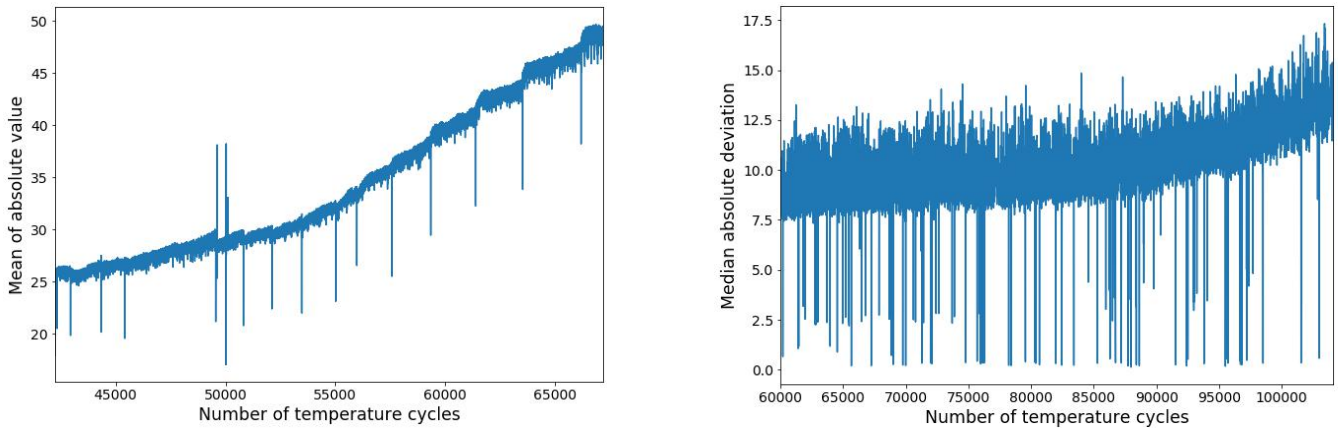

(a) (b)

Fig. 12 Features without preprocessing. (a) Mean of absolute value of IGBT1 (b) Median absolute deviation of IGBT2

The features after the abnormal points are deleted are shown in Fig 13. The trend of two features that are the most relevant to the number of cycles is illustrated in the figures. For IGBT1 IGBT2, and IGBT3 both mean of absolute value (MAV) and median absolute deviation (MAD) increase as the aging time becomes longer. For the fourth IGBT, the features also change slowly during the aging process.

However, the features showed a sharp change at about the 58300th cycle due to the breakage of the bonding wire of the module. Observed from the failure pictures, the bond wire fracture is caused by the local high temperature causing the wire to fuse rather than fatigue crack propagation. No matter which kind of bonding wire fails, we can monitor it from the transient thermal resistance curve.

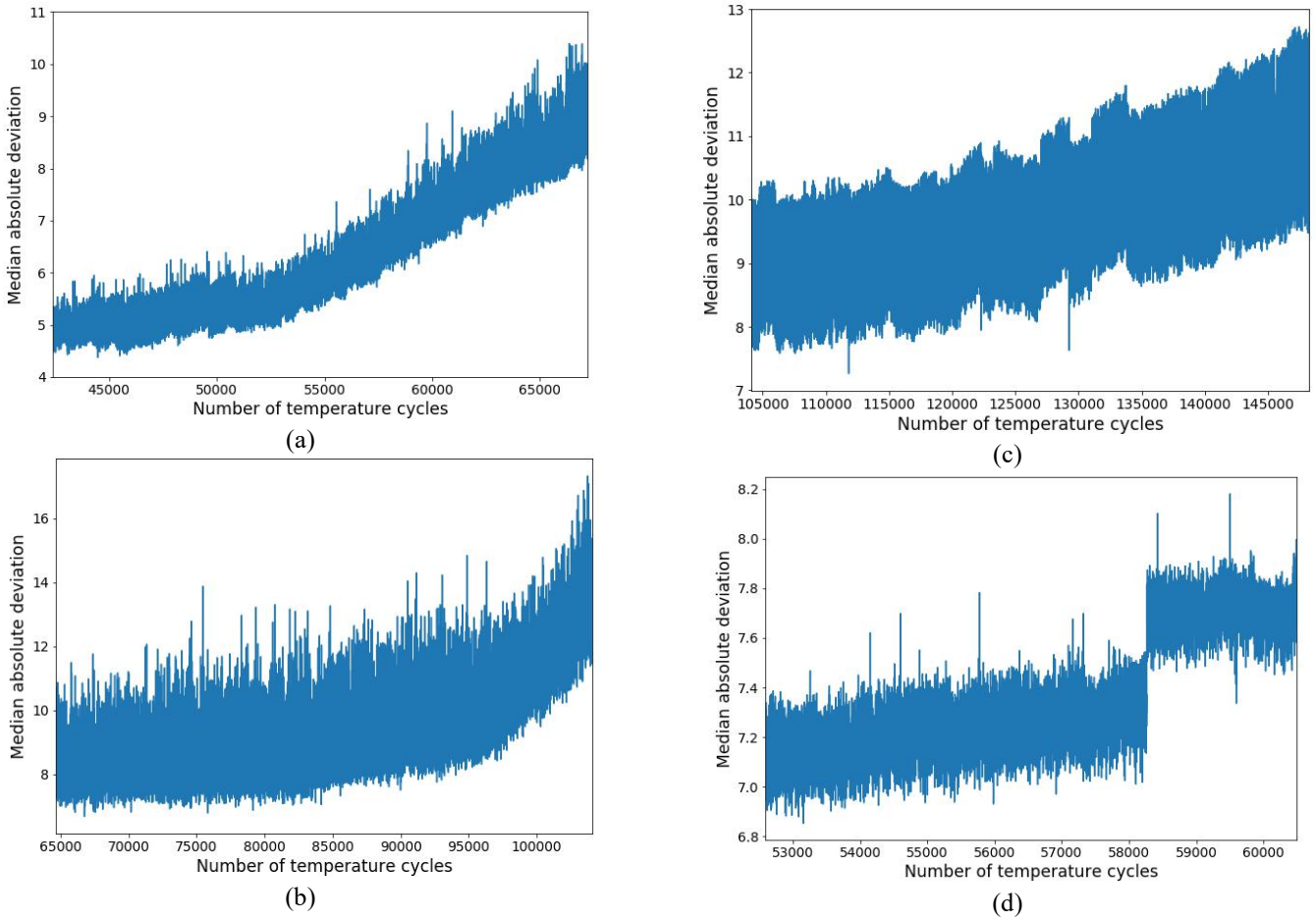

(a) (c)

(b) (d)

Fig. 13 Median absolute deviation of different IGBT modules. (a) IGBT1 (b) IGBT2 (c) IGBT3 (d)IGBT4

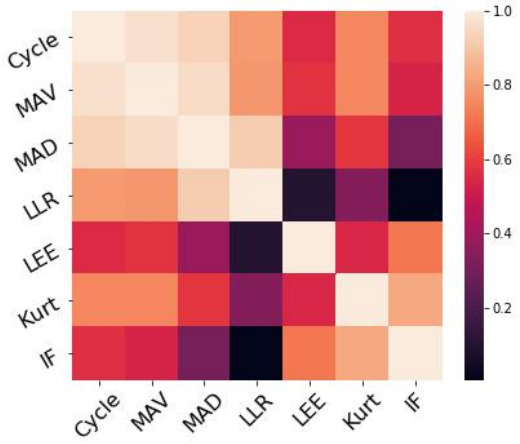

Fig. 14 Correlations of different features.

Not all features calculated from the IGBT transient thermal impedance curve are sensitive to describe the status of the IGBT. We first eliminate the features whose correlation coefficients are lower than 0.6. Among the remaining features related to the life of the IGBT, many features that have a correlation coefficient higher than 0.9 with each other. We also filter them out as redundant data. Finally, the features of the life prediction method used in this study are as follows: the mean absolute deviation, the mean of absolute value, the kurtosis, the impulse factor, the log-log ratio, the log energy entropy. Therefore, 6 features are extracted from each transient thermal impedance curve. The correlation between cycle number and feature is shown in Fig.14.

B. RUL Prediction

After feature extraction, we divide the data into a training set and test set. Since the transient thermal impedance has almost no change for a long time in the aging data, we only use the last piece of data in the aging data as the data set. For the aging data of IGBT1, the last 25000 cycles are used and the last 13000 cycles are used as the test dataset. As for IGBT2, we use the last 13000 cycles as dataset and the last 6000 cycles as the test dataset. For IGBT3, the last 40000 cycles are used and the last 18000 cycles are used as test dataset. When training the model, the data of 100 cycles before the ith cycle are input into the model that outputs RUL of the ith cycle. The root mean square error (RMS) of the predicted life and the actual life is used as the loss function to optimize the model. The final prediction results are shown in Fig. 15.

TABLE III
MAE comparison

	Attention	LSTM
IGBT1	208	308
IGBT2	139	304
IGBT3	184	285

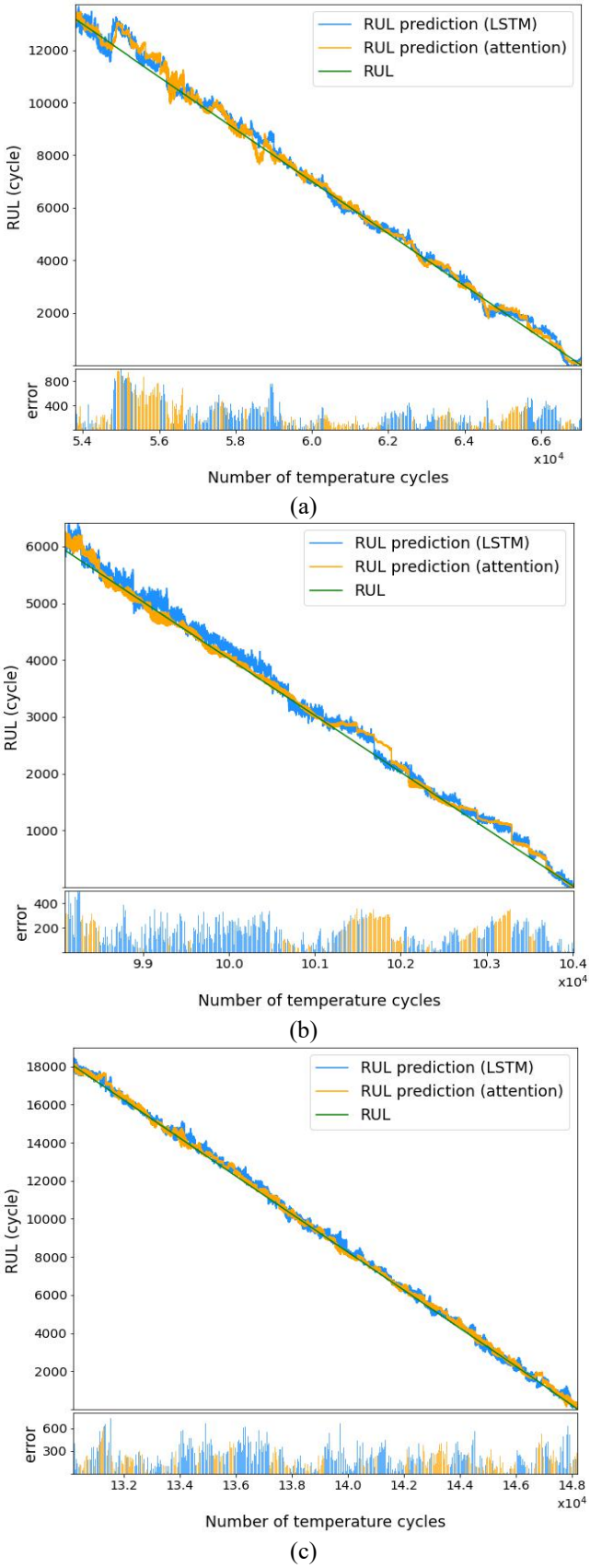

Fig. 15 RUL prediction results. (a) IGBT1 (b) IGBT2 (c)IGBT3

In order to prove the advantage of the proposed model, we also established an LSTM model which has the same structure but no attention mechanism to predict RUL. Fig.15 shows the prediction results of two different models. Bar charts on the bottom of the figures indicate the absolute errors of two different models. They are distinguished by different colors and the error with larger values is shown. Mean absolute error (MAE) is used to evaluate the performance. As shown in TABLE III, the MAE of the model with attention mechanism is smaller than the LSTM model.

The features of the transient thermal impedance proposed in this paper are not so sensitive to temperature like other aging parameters such as $V_{ce,on}$. Although the junction temperature is measured by thermocouples in this paper, which is not practical in actual working conditions, the method of junction temperature measurement is well developed in recent years and does not require additional expensive or complicated measuring system[31-33]. In short, the method of using attention neural network proposed to use the data of IGBT transient thermal impedance to predict the remaining life of IGBT has high accuracy and feasibility.

V. Conclusion

As IGBTs become more and more widely used, how to estimate the remaining life of the module to assist in maintenance has become an issue of great concern in the actual working environment. This paper proposes a method to predict the remaining life of IGBT using the attention model based on the features of the transient thermal impedance. Firstly, by conducting the aging test of the IGBT, we found that the transient thermal impedance of the module changes with the aging of the IGBT. Based on this phenomenon, we extract the characteristics of transient thermal impedance and use neural network methods to predict the remaining life of the IGBT. The results show that the attention neural network can predict the remaining life precisely. The main contribution of this study is to identify the effectiveness of the features of the transient thermal impedance as the aging precursor. Another contribution is to establish a neural network with attention mechanism to predict the RUL precisely. Although collecting temperature by thermocouples is impractical, other methods of temperature measurement can be used to realize the proposed approach in the practical scenario.

References

[1] J. Ribrant and L. Bertling, "Survey of failures in wind power systems with focus on Swedish wind power plants during 1997-2005," in *2007 IEEE Power Engineering Society General Meeting, PES*, Tampa, FL, 2007.

[2] S. Yang, A. Bryant, P. Mawby, D. Xiang, L. Ran, and P. Tavner, "An industry-based survey of reliability in power electronic converters," *IEEE Transactions on Industry Applications,* Article vol. 47, no. 3, pp. 1441-1451, 2011, Art. no. 5729810.

[3] O. A. Plekhov, N. Saintier, T. Palin-Luc, S. V. Uvarov, and O. B. Naimark, "Theoretical analysis, infrared and structural investigations of energy dissipation in metals under cyclic loading," (in English), *Materials Science and Engineering A,* Article vol. 462, no. 1-2, pp. 367-369, 2007.

[4] C. Basaran and R. Chandaroy, "Finite element simulation of the temperature cycling tests," (in English), *IEEE Transactions on Components Packaging and Manufacturing Technology Part A,* Article vol. 20, no. 4, pp. 530-536, 1997.

[5] J. M. Thébaud, E. Woirgard, C. Zardini, S. Azzopardi, O. Briat, and J. M. Vinassa, "Strategy for designing accelerated aging tests to evaluate IGBT power modules lifetime in real operation mode," *IEEE Transactions on Components and Packaging Technologies,* Article vol. 26, no. 2, pp. 429-438, 2003.

[6] D. Astigarraga *et al.*, "Analysis of the Results of Accelerated Aging Tests in Insulated Gate Bipolar Transistors," *IEEE Transactions on Power Electronics,* Article vol. 31, no. 11, pp. 7953-7962, 2016, Art. no. 7368210.

[7] S. H. Ali, S. Dusmez, and B. Akin, "Investigation of collector emitter voltage characteristics in thermally stressed discrete IGBT devices," in *2016 IEEE Energy Conversion Congress and Exposition, ECCE 2016*, 2016: Institute of Electrical and Electronics Engineers Inc.

[8] O. Schilling, M. Schäfer, K. Mainka, M. Thoben, and F. Sauerland, "Power cycling testing and FE modelling focussed on Al wire bond fatigue in high power IGBT modules," *Microelectronics Reliability,* Article vol. 52, no. 9-10, pp. 2347-2352, 2012.

[9] Z. Liu, W. Mei, X. Zeng, C. Yang, and X. Zhou, "Remaining useful life estimation of insulated gate biploar transistors (IGBTS) based on a novel volterra K-nearest neighbor optimally pruned extreme learning machine (VKOPP) model using degradation data," *Sensors (Switzerland),* Article vol. 17, no. 11, 2017, Art. no. 2524.

[10] V. Smet *et al.*, "Ageing and failure modes of IGBT modules in high-temperature power cycling," *IEEE Transactions on Industrial Electronics,* Article vol. 58, no. 10, pp. 4931-4941, 2011, Art. no. 5711661.

[11] U. M. Choi, S. Jørgensen, F. Iannuzzo, and F. Blaabjerg, "Power cycling test of transfer molded IGBT modules by advanced power cycler under different junction temperature swings," (in English), *Microelectronics Reliability,* Article vol. 88-90, pp. 788-794, 2018.

[12] F. Forest, A. Rashed, J. J. Huselstein, T. Martiré, and P. Enrici, "Fast power cycling protocols implemented in an automated test bench dedicated to IGBT

module ageing," *Microelectronics Reliability,* Article vol. 55, no. 1, pp. 81-92, 2015.

[13] M. Held, P. Jacob, G. Nicoletti, P. Scacco, and M. H. Poech, "Fast power cycling test for IGBT modules in traction application," 1997, vol. 1, pp. 425-430.

[14] N. Patil, J. Celaya, D. Das, K. Goebel, and M. Pecht, "Precursor parameter identification for insulated gate bipolar transistor (IGBT) prognostics," (in English), *IEEE Transactions on Reliability,* Article vol. 58, no. 2, pp. 271-276, 2009.

[15] M. S. Haque, M. N. B. Shaheed, and S. Choi, "RUL Estimation of Power Semiconductor Switch using Evolutionary Time series Prediction," in *2018 IEEE Transportation and Electrification Conference and Expo, ITEC 2018*, 2018, pp. 564-569.

[16] M. S. Haque, S. Choi, and J. Baek, "Auxiliary particle filtering-based estimation of remaining useful life of IGBT," *IEEE Transactions on Industrial Electronics,* Article vol. 65, no. 3, pp. 2693-2703, 2018, Art. no. 8012424.

[17] S. H. Ali, M. Heydarzadeh, S. Dusmez, X. Li, A. S. Kamath, and B. Akin, "Lifetime Estimation of Discrete IGBT Devices Based on Gaussian Process," (in English), *IEEE Transactions on Industry Applications,* Conference Paper vol. 54, no. 1, pp. 395-403, 2018, Art. no. 8039225.

[18] S. H. Ali, E. Ugur, and B. Akin, "Analysis of Vth Variations in IGBTs under thermal stress for improved condition monitoring in automotive power conversion systems," (in English), *IEEE Transactions on Vehicular Technology,* Article vol. 68, no. 1, pp. 193-202, 2019, Art. no. 8532311.

[19] A. Alghassi, S. Perinpanayagam, M. Samie, and T. Sreenuch, "Computationally efficient, real-time, and embeddable prognostic techniques for power electronics," *IEEE Transactions on Power Electronics,* Article vol. 30, no. 5, pp. 2623-2634, 2015, Art. no. 6915717.

[20] S. Zhou, L. Zhou, and P. Sun, "Monitoring potential defects in an IGBT module based on dynamic changes of the gate current," *IEEE Transactions on Power Electronics,* Article vol. 28, no. 3, pp. 1479-1487, 2013, Art. no. 6266754.

[21] M. Held, P. Jacob, G. Nicoletti, P. Scacco, and M. H. Poech, "Fast power cycling test for insulated gate bipolar transistor modules in traction application," *International Journal of Electronics,* Article vol. 86, no. 10, pp. 1193-1204, 1999.

[22] M. Bouarroudj, Z. Khatir, J. P. Ousten, F. Badel, L. Dupont, and S. Lefebvre, "Degradation behavior of 600 V-200 A IGBT modules under power cycling and high temperature environment conditions," *Microelectronics Reliability,* Article vol. 47, no. 9-11 SPEC. ISS., pp. 1719-1724, 2007.

[23] B. Ji *et al.*, "In situ diagnostics and prognostics of solder fatigue in IGBT modules for electric vehicle drives," *IEEE Transactions on Power Electronics,* Article vol. 30, no. 3, pp. 1535-1543, 2015, Art. no. 6804693.

[24] X. Cao, T. Wang, K. D. T. Ngo, and G. Q. Lu, "Characterization of lead-free solder and sintered nano-silver die-attach layers using thermal impedance," *IEEE Transactions on Components, Packaging and Manufacturing Technology,* Article vol. 1, no. 4, pp. 495-501, 2011, Art. no. 5729793.

[25] M. Du, Q. Guo, Z. Ouyang, K. Wei, and W. G. Hurley, "Effect of solder layer crack on the thermal reliability of Insulated Gate Bipolar Transistors," *Case Studies in Thermal Engineering,* Article vol. 14, 2019, Art. no. 100492.

[26] S. Hochreiter and J. Schmidhuber, "Long Short-Term Memory," (in English), *Neural Computation,* Article vol. 9, no. 8, pp. 1735-1780, 1997.

[27] A. Vaswani *et al.*, "Attention is all you need," 2017, vol. 2017-December, pp. 5999-6009: Neural information processing systems foundation.

[28] C. C. Chiu *et al.*, "State-of-the-Art Speech Recognition with Sequence-to-Sequence Models," in *2018 IEEE International Conference on Acoustics, Speech, and Signal Processing, ICASSP 2018*, 2018, vol. 2018-April, pp. 4774-4778.

[29] S. Ren, K. He, R. Girshick, and J. Sun, "Faster R-CNN: Towards Real-Time Object Detection with Region Proposal Networks," *IEEE Transactions on Pattern Analysis and Machine Intelligence,* Article vol. 39, no. 6, pp. 1137-1149, 2017, Art. no. 7485869.

[30] J. R. Jiang, J. E. Lee, and Y. M. Zeng, "Time series multiple channel convolutional neural network with attention-based long short- term memory for predicting bearing remaining useful life," (in English), *Sensors (Switzerland),* Article vol. 20, no. 1, 2020, Art. no. 166.

[31] V. Smet, F. Forest, J. J. Huselstein, A. Rashed, and F. Richardeau, "Evaluation of Vce monitoring as a real-time method to estimate aging of bond wire-IGBT modules stressed by power cycling," *IEEE Transactions on Industrial Electronics,* Article vol. 60, no. 7, pp. 2760-2770, 2013, Art. no. 6191320.

[32] J. Hu, M. Huang, Y. Liu, and X. Zha, "Transient junction temperature estimation of IGBT using improved thermal model," *Microelectronics Reliability,* Article vol. 88-90, pp. 1146-1150, 2018.

[33] M. A. Eleffendi and C. M. Johnson, "Application of Kalman Filter to Estimate Junction Temperature in IGBT Power Modules," *IEEE Transactions on Power Electronics,* Article vol. 31, no. 2, pp. 1576-1587, 2016, Art. no. 7073633.